Full waveform inversion using the PSPI migration: a convergence study

Marcelo Guarido*, Laurence Lines*, Robert Ferguson†

ABSTRACT

A full waveform inversion (FWI) routine using PSPI migration with a deconvolution imaging condition was tested on an acoustic synthetic 2D survey using the Marmousi model. Inverted P-wave velocities are, in the worst case, promising. The model update is computed by averaging monochromatic scaled gradients at each iteration and the resulting model is an improvement of the one obtained in the previous work Guarido et al. (2014). We tested different starting models to check the routine behavior and, as expected, better the initial model, better will be the migration of the residuals and the model update, resulting in higher resolution velocity inversion. The conjugate gradient was included in the routine, building more precise gradients and increasing the quality of the inverted model. Impedance inversion by trace integration was applied in the model update (gradient) showing promising results, mostly related to the inversion of thicker layers, but it still requires improvement.

INTRODUCTION

Seismic inversion techniques are the ones that use intrinsic informations contained in the data to determine rock properties by matching a model that "explains" the data. Some examples are the variation of amplitude per offset, or AVO (Shuey, 1985; Fatti et al., 1994), the traveltime differences between traces, named traveltime tomography (Langan et al., 1984; Bishop and Spongberg, 1984; Cutler et al., 1984), or even by matching synthetic data to the observed data, as it is done in full waveform inversion (Tarantola, 1984; Virieux and Operto, 2009; Margrave et al., 2010; Pratt et al., 1998), among others. These inversions can compute rock parameters as P and S waves velocities, density, viscosity and others. In this work we are focused in the inversion of the P wave velocity.

FWI, is a least-square based inversion, which objective is to find the model parameters that minimizes the difference between observed (acquired) data and synthetic shots (Margrave et al., 2011), or the residuals. This is accomplished in an iterative fit method by linearizing a non-linear problem.

The full waveform inversion was proposed in the early 80's (Pratt et al., 1998) but the technique was considered too expensive in computational terms. Lailly (1983) and Tarantola (1984) simplified the methodology by using the steepest-descent method (or gradient method) in the time domain to minimize the objective function without calculate, explicitly, the partial derivatives. They compute the gradient by a reverse-time migration (RTM) of the residuals. Pratt et al. (1998) develop a matrix formulation for the full waveform inversion in the frequency domain and present efficient ways to compute the gradient and

*CREWES - University of Calgary
†Orthogonal Geophysics

the inverse of the Hessian matrix (the step length for convergence in the FWI) the Gauss-Newton or the Newton approximations. The FWI is shown to be more efficient if applied in a multi-scale method, where lower frequencies are inverted first and is increased as more iterations are done (Pratt et al., 1998; Virieux and Operto, 2009; Margrave et al., 2010). An overview of the FWI theory and studies are compiled by Virieux and Operto (2009). Lindseth (1979) showed that an impedance inversion from seismic data is not effective due to the lack of low frequencies during the acquisition but could be compensated by the match with a sonic-log profile. Margrave et al. (2010) used a gradient method and matched it with sonic logs profiles to compensate the absence of the low frequency and to calibrate the model update by computing the step length and a phase rotation (avoiding cycle skipping). They also proposed the use of a PSPI (phase-shift-plus-interpolation) migration (Ferguson and Margrave, 2005) instead of the RTM, so the iterations are done in time domain but only selected frequency bands are migrated, using a deconvolution imaging condition (Margrave et al., 2011; Wenyong et al., 2013) as a better reflectivity estimation. Warner and Guasch (2014) use the deviation of the Weiner filters of the real and estimated data as the object function with great results.

We are applying the FWI methodology using the PSPI migration Margrave et al. (2010); Ferguson and Margrave (2005) with a deconvolution imaging condition to compute the gradient. A conjugate gradient is also used to improve the quality of the gradient and to reduce the number of iterations (Zhou et al., 1995; Vigh and Starr, 2008). The step length is computed by a least-square minimization (Pica et al., 1990) and is being estimated for individual frequencies. The synthetic data is done by a finite difference forward modelling algorithm.

THEORY

The steepest-descent method

The objective function of the FWI method is, in general:

$$C(\mathbf{m}) = ||\mathbf{d}_0 - \mathbf{d}(\mathbf{m})||^2 = ||\Delta\mathbf{d}(\mathbf{m})||^2 \tag{1}$$

where Δd is the data residual, m is the model and $||$ represents the norm-2 of the array. The minimization is done by doing a Taylor's expansion of the objective function of the equation 1 around a perturbation in the model δm and taking the derivative equal to zero (Tarantola, 1984; Pratt et al., 1998; Virieux and Operto, 2009). The solution is:

$$\mathbf{m}_{n+1} = \mathbf{m}_n + H_n^{-1}\mathbf{g}_n \tag{2}$$

where H is the Hessian, g is the gradient computed by back-propagating the data residual and n is the *n-th* iteration. It is known as the Newton method. For the steepest-descent method, the Hessian matrix can be neglected and be equalized to the identity matrix:

$$\mathbf{m}_{n+1} = \mathbf{m}_n + \alpha_n \mathbf{g}_n \tag{3}$$

where α is the step length (the scale factor). Here, the gradient is understood to be the PSPI migrated residuals with a deconvolution imaging condition (Margrave et al., 2010, 2011; Wenyong et al., 2013; Guarido et al., 2014).

In this work we are proposing to compute the gradient as the stack of the scaled gradient per each frequency. This way, equation 3 can be written as:

$$\mathbf{m}_{n+1} = \mathbf{m}_n + \frac{1}{N}\sum_{i=1}^{N} \alpha_n(\omega_i)\mathbf{g}_n(\omega_i) \tag{4}$$

where ω_i is the *i-th* frequency in the total of *N* frequencies used to compute the gradient. The early iterations uses very low frequencies only ($\approx 2 - 4Hz$) and next iterations have the lower frequency fixed and the maximum frequency of the range increased. This means that, for each iterations, *N* migrations are computed. The step length α will be computed for each frequency prior the stack. This way we expect a flatter gradient spectrum.

Step length computation

Pica et al. (1990) computed the step length (scale factor) by minimizing the objective function:

$$C(\mathbf{m_{n+1}}) = C(\mathbf{m}_n + \alpha_n \mathbf{g}_n) = \left[\mathbf{d}_0 - \mathbf{d}\left(\mathbf{m}_n + \alpha_n \mathbf{g}_n\right)\right]^T \left[\mathbf{d}_0 - \mathbf{d}\left(\mathbf{m}_n + \alpha_n \mathbf{g}_n\right)\right] \tag{5}$$

We also have:

$$\mathbf{F}\delta\mathbf{m} = \lim_{\epsilon \to 0} \frac{\mathbf{g}(\mathbf{m} + \epsilon\delta\mathbf{m}) - \mathbf{g}(\mathbf{m})}{\epsilon} \tag{6}$$

where $\mathbf{F}$ is an operator that takes the derivative of $\mathbf{d}$ at the point $\mathbf{m}$ and $\delta\mathbf{m}$ is the perturbation in the model.

Equation 5 can be written as:

$$C(\mathbf{m_{n+1}}) = \left[\mathbf{d}_0 - \mathbf{d}\left(\mathbf{m}_n\right) + \alpha_n \mathbf{F}_n \mathbf{g}_n\right]^T \left[\mathbf{d}_0 - \mathbf{d}\left(\mathbf{m}_n\right) + \alpha_n \mathbf{F}_n \mathbf{g}_n\right] \tag{7}$$

Minimizing equation 7 relative to α_n (taking the derivative and making it equals to zero), leads to the optimal α_n:

$$\alpha_n = \frac{\left[\mathbf{F}_n\mathbf{g}_n\right]^T\left[\mathbf{d}_0 - \mathbf{d}\left(\mathbf{m}_n\right)\right]}{\left[\mathbf{F}_n\mathbf{g}_n\right]^T\left[\mathbf{F}_n\mathbf{g}_n\right]} \tag{8}$$

This reduce the problem for the step length to a single forward modelling in a perturbation in the velocity model $\mathbf{m} = \mathbf{m}_n + \epsilon\mathbf{g}_n$ and is cheaper than a step length computed by a line search (Guarido et al., 2015).

For our tests, computation of the step of equation 8 is done using a single reference shot (the one in the center of the velocity model).

The conjugate gradient

Equation 3 can be rewritten replacing the gradient $\mathbf{g}_n$ by the conjugate gradient $\mathbf{h}_n$ (Zhou et al., 1995; Vigh and Starr, 2008; Ma et al., 2010):

$$\mathbf{m}_{n+1} = \mathbf{m}_n + \alpha_n\mathbf{h}_n \tag{9}$$

where

$$\mathbf{h}_0 = \mathbf{g}_0, \beta_n = \frac{\mathbf{g}_n^T\left(\mathbf{g}_n - \mathbf{g}_{n-1}\right)}{\mathbf{g}_{n-1}^T\mathbf{g}_{n-1}}, \mathbf{h}_n = \mathbf{g}_n + \beta_n\mathbf{h}_{n-1} \tag{10}$$

Impedance inversion

Mostly of the tests in this paper are done using the pure migration output (reflection coefficients) as the model update once we use very low frequencies (starting in $2Hz$). However the FWI theory implies in a type of trace integration during the gradient computation. In other words, an impedance inversion should be applied (Margrave et al., 2010, 2011).

For normal incident P-waves, the reflection coefficients due to impedance contrast in the interface of two mediums is (Treitel et al., 1995):

$$R_i = \frac{\rho_{i+1}V_{i+1} - \rho_i V_i}{\rho_{i+1}V_{i+1} + \rho_i V_i} \tag{11}$$

where R_i is the reflection coefficient on the ith interface, ρ is the density and V is the P wave velocity propagation. The multiplication of density and velocity is the acoustic impedance I_i. For small contrasts of acoustic impedances in geological interfaces (usually < 0.3), equation 11 can be written:

$$R_i = \frac{\Delta I_i}{2I_i} \tag{12}$$

Assuming the reflection sequence as continuous in time, and taking the limit $\Delta_t \to 0$:

$$R(t) = \frac{1}{2} d\left(\ln I(t)\right) \tag{13}$$

Integrating over time and assuming constant density:

$$V(t) = V_0 e^{2\int_{t_1}^{t} R(\tau) d\tau} \tag{14}$$

The gradient can be inverted from reflection coefficients to impedance by taking the exponential of the integrated trace.

RESULTS

The initial model

The synthetic test is done in the Marmousi model (figure 1). Pilot shots (used as the real shots), were created using an acoustic finite difference algorithm. In the total, 102 shots are used to simulate field data. Shot spacing is 100m. Each shot has a maximum of 401 receivers (varying in the edges of the model) totalizing 2000m of maximum offset. The register time is 3s and sample rating of 4ms (figure 2). The dominant frequency of the wavelet is 5Hz.

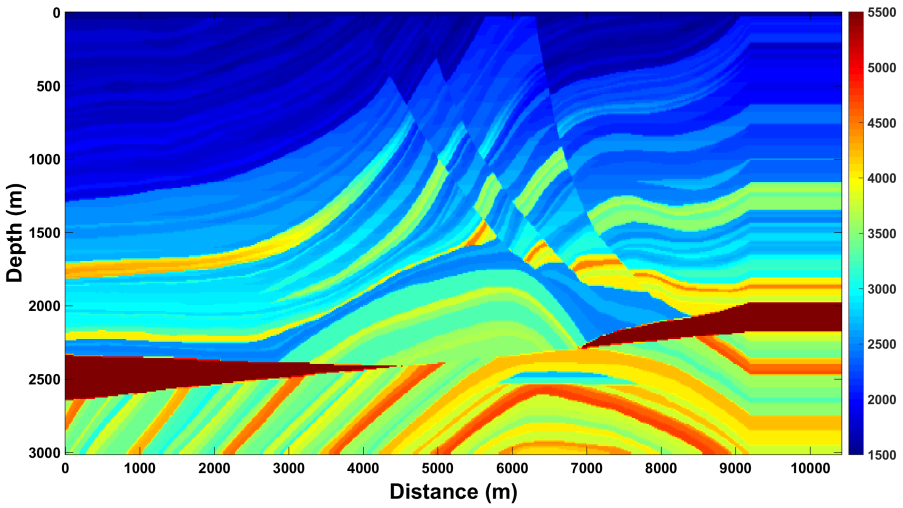

FIG. 1. The Marmousi 2D model. The color bar indicates the wave propagation velocity in m/s.

During the FWI routine, synthetic shots are created with the same finite difference forward modeling algorithm, wavelet and acquisition parameters as pilot shots. They differ from each other by the velocity model used and the routine starts using a guessing model, usually a depth migration velocity (Virieux and Operto, 2009). The residuals (difference between real and synthetic shot) is then migrated with the PSPI migration with a deconvolution imaging condition. For the first iterations, only very low frequency are used ($2-4Hz$),

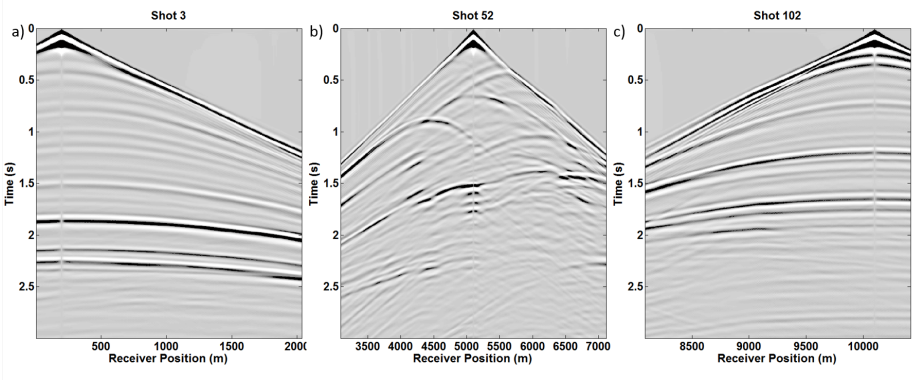

FIG. 2. Three of the 102 shots used in the test. a) shot 3, b) shot 52 and c) shot 102.

and the frequency range is increased by $2Hz$ when errors are stable (variation of the 3 last iterations is less than 0.1%). Each frequency is migrated independently, i.e., for the range of $2-4Hz$ three migrations are necessary. This is done for each residuals. All the migrated residuals are muted (Guarido et al., 2014), stacked (creating one gradient per frequency) and smoothed (Margrave et al., 2010; Guarido et al., 2014). For now, an impedance inversion is not applied. The step length is calculated using equation 8 for each monochromatic gradient. The final gradient is the average (equation 4) of all scaled monochromatic gradients and it is used to update the model for the next iteration.

For the initial guess test the gradient is estimated using equation 4 (the conjugate gradient is not estimated in this test). Three different initial guesses are tested (figure 3). All the models are a convolution of the Marmousi model of figure 1 with a Gaussian window. Each of the initial models represents a different challenge of the routine, where the model of figure 3a is a starting model closer to the global minimum, the model of figure 3c is more challenging (and is the main initial model for all the others tests) and the model of figure 3e contains only trends of the Marmousi model.

Figure 3 also presents the inversion results using the correspondent initial model. It is notable that better (closer to the global minimum) the initial model is, better will be inverted model. This can be explained by the quality of the migration since the first iteration. The interfaces are migrated closer to the correct position and inversion has a higher change to converge to the global minimum. Figure 3b is a higher resolution model that contains mostly characteristics of the Marmousi model (figure 1) and is a remarkable result. When the initial guess starts to get far from the global minimum (as figures 3c and 3e), the inverted model loses resolution. However, the velocity models of figures 3d and 3d are still impressive (the model of figure 3d has, mostly, equal or more features than the good initial guess of figure 3a). We are confident that all the final models can be used as migration velocity.

The next step is to use the resulted models of figure 3 as migration velocities. A prestack depth migration (in here the same PSPI code) is used to migrate each shot and then stacked. Figure 4a is the migrated section using the Marmousi model (slightly smoothed) as migration velocity. The figures 4b, 4c and 4d are migrated sections using velocities of figures 3b, 3d and 3f, respectively. Again, better the model, the migrated section using an

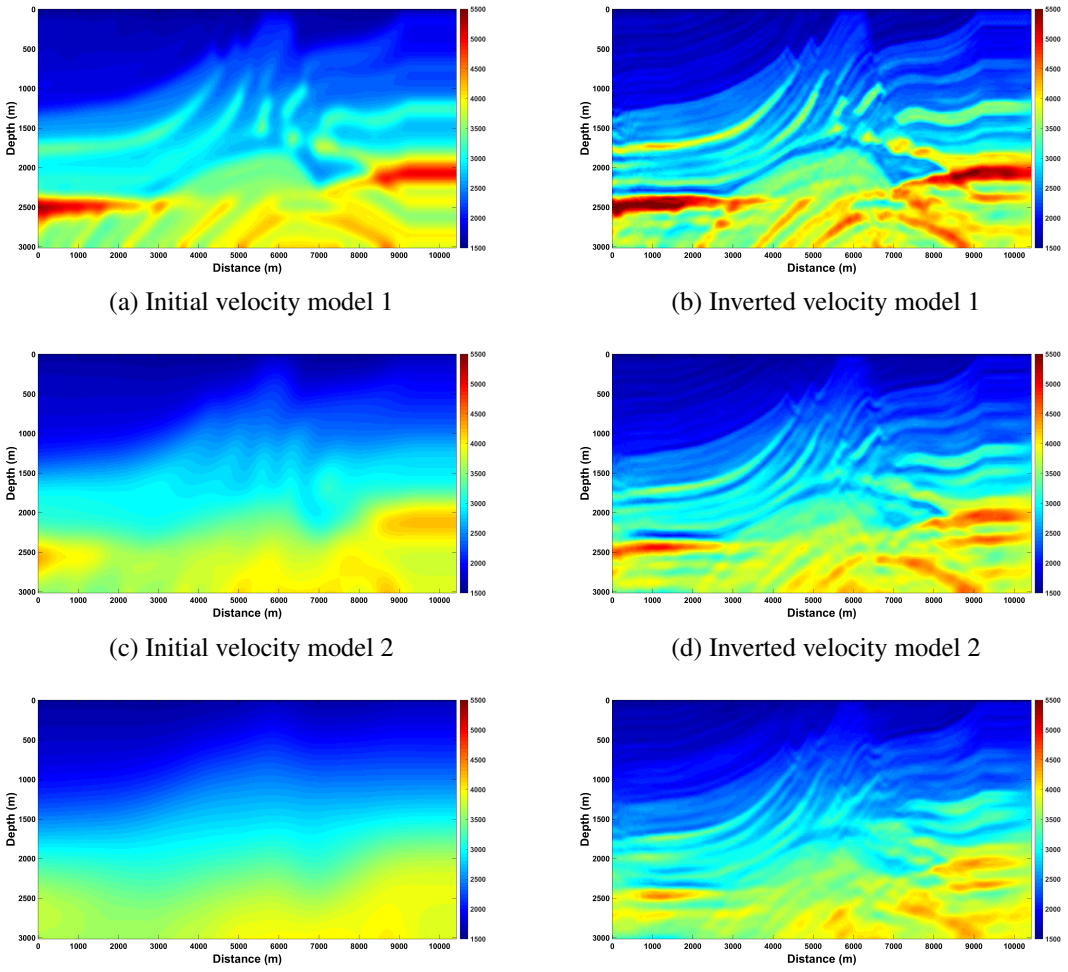

(a) Initial velocity model 1

(b) Inverted velocity model 1

(c) Initial velocity model 2

(d) Inverted velocity model 2

(e) Initial velocity model 3

(f) Inverted velocity model 3

FIG. 3. The tested initial velocity guesses. All of them is the original Marmousi model convolved is a different Gaussian window.Also the inverted models. Closer to the global minimum the initial guess is, better is the inverted model.

inverted velocity converge to the real solution.

Convergence is checked on figure 5a, where errors (normalized $norm - 2$) of the reference shot is computed per iteration. For the three tests, errors decrease at each iteration until stability is reached at maximum frequency of $61Hz$. It is visible how the error decreases as we start inverting with an initial guess that is closer to the global minimum. When analyzing figure 5b, we see similar behavior as the shot errors. The difference is on model 2 (blue line) minimum at iteration 34, suggesting that the shot errors can be only in mostly cases a good reference for the model global minimum.

Figure 6 is the 1D plot of the center row of the real, initial and inverted model for all the three tested models. In the left is the inversion using the best initial model and the final answer gets closer to the real one. As the initial guess gets far of the global minimum (center and right plots) we can still get a very good answers, but they also increase the

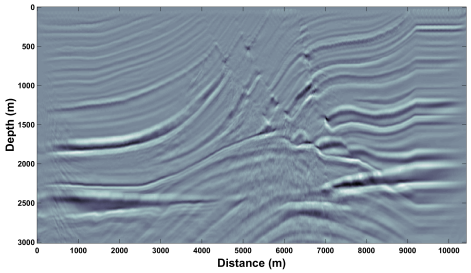

(a) Migrated shots using Marmousi model

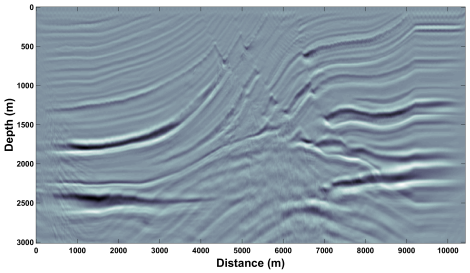

(b) Migrated shots using model of figure 3b

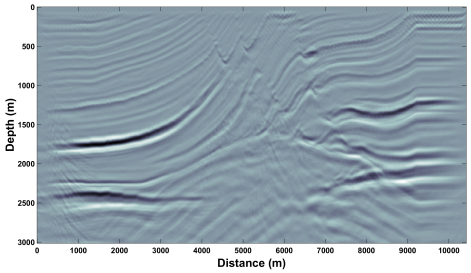

(c) Migrated shots using model of figure 3d

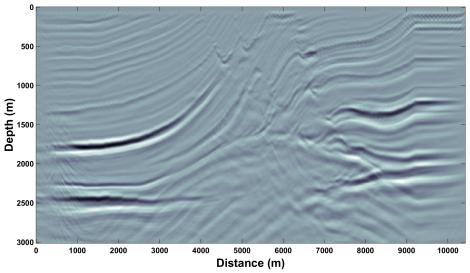

(d) Migrated shots using model of figure 3f

FIG. 4. Migrated shots using the inverted models of figure 3. Better the model, higher is the migration quality.

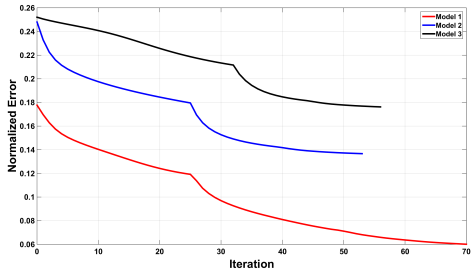

(a) Shot errors

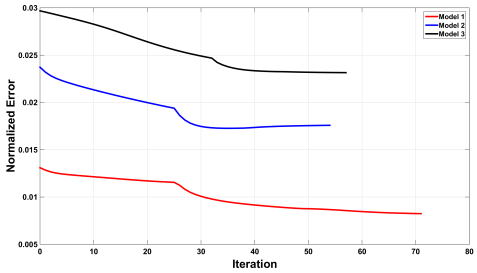

(b) Model errors

FIG. 5. Errors ($norm - 2$) of the inversions for each initial model. a) are the errors related to real synthetic reference shots and b) is the error of the inverted model of each iteration when compared to the Marmousi model.

distance to the global minimum. It is good to point that all the inverted models look to a smoothed version of the Marmousi model and, as showed before, they are good migration velocities.

Application of the conjugate gradient

Now the conjugate gradient is estimated using equation 10 and model is updated according to equation 9. Impedance inversion is not applied yet.

We used the same routine as we used on previous section, but the conjugate gradient is

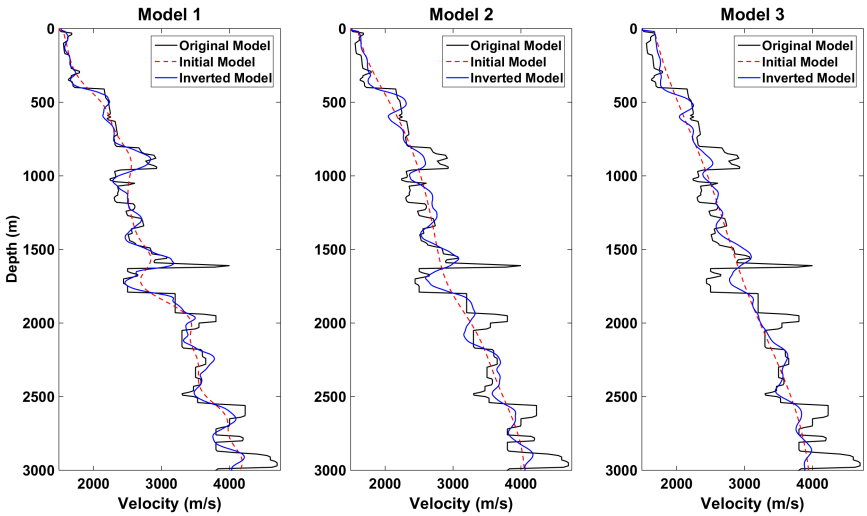

FIG. 6. The 1D plot of the center row of the real, initial and inverted model for all the three tested models. Better the initial guess is, better will be the inverted model.

computed after the scaled monochromatic gradients are stacked (or averaged). Figure 7 is the inverted model using as starting model the smoothed version of the Marmousi model as showed on figure 3c. Conjugate gradient improved the inversion quality if compared with the "classic" gradient one (figure 3d).

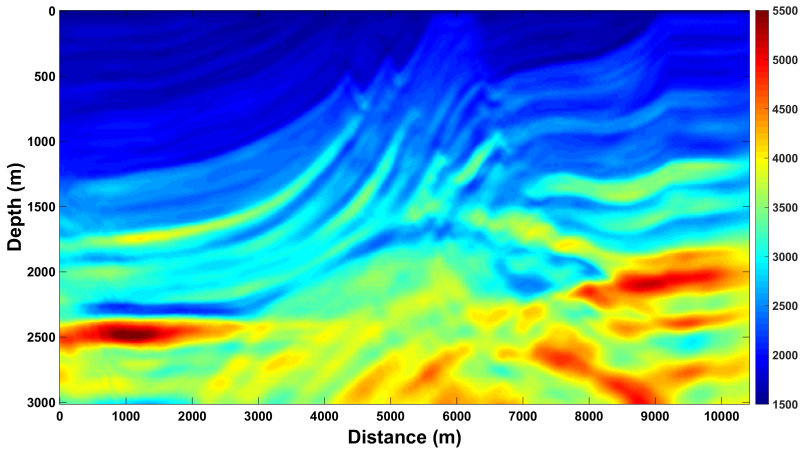

FIG. 7. Inverted model using the conjugate gradient. The initial guess is the one on figure 3c. The final model has higher resolution than the model of figure 3d.

Reference shot errors (normalized $norm - 2$) of the conjugate gradient inversion (red line) is compared with the errors of the classic gradient inversion (blue line) on figure 8a. Both lines have a very close "path" until iteration 52, when the classic gradient stabilized while the conjugate gradient kept updating the model and reducing the error for 10 more iterations. This indicates that the conjugate gradient could take more advantage while inverting higher frequencies providing a final model with improved quality. However the real improvement of the conjugate gradient can be easily checked on figure 8b. The error of the models per iteration shows that the conjugate gradient leads the inversion closer to the

global minimum. This is a very important observation, as the conjugate gradient strongly increase inversion resolution with a insignificant computational cost.

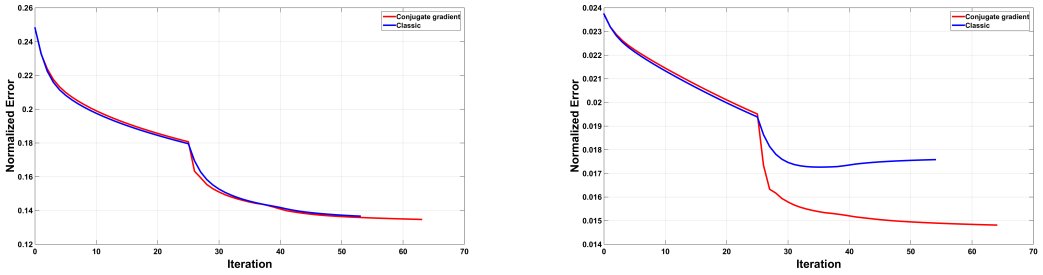

(a) Shot errors (b) Model errors

FIG. 8. Errors ($norm - 2$) of the inversions for each initial model. a) are the errors related to real synthetic reference shots and both classic and conjugate gradient show very similar behavior, and b) is the error of the inverted model of each iteration when compared to the Marmousi model, and it is clear how the conjugate gradient improves the inversion resolution.

Figure 9 is the 1D plot of the center row of the real, initial and inverted model comparing classic and conjugate gradients. Both inversions look close to each other. However, the conjugate gradient inversion (red dashed line) looks slightly closer to the Marmousi model (black line). As it was discussed before, the conjugate gradient method improves the inverted model if compared to the classic one.

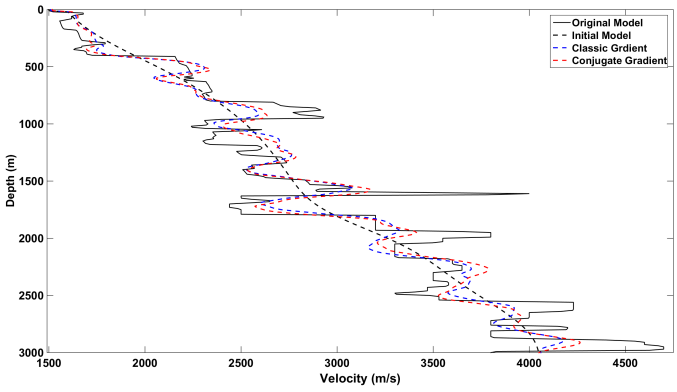

FIG. 9. The 1D plot of the center row of the real, initial and inverted model comparing classic and conjugate gradients. Both inversions have close behavior, but the conjugate gradient inversion shows a slightly better (closer to the real model) result.

Analyzing the migrated section of the figure 10b that used as velocity model the conjugate gradient inversion, there is significant difference when compared with the migrated section that used the classic gradient inversion as velocity model. Shallow structures are clearer, are in a more correct position and deep layers are less shifted when compared with the migration using Marmousi velocity of figure 10a.

The conjugate gradient is cheap to be applied and results in a great improvement of the inversion quality. It increases the number of iterations to finish the inversion because stop criteria is not reached, meaning that it keeps improving the model for a longer period.

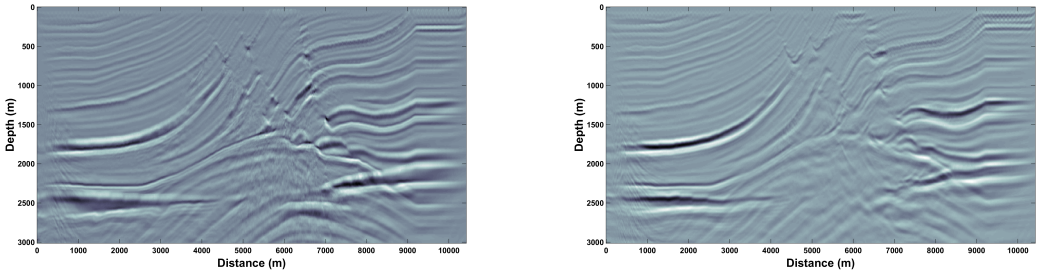

(a) Migrated shots using Marmousi model (b) Migrated shots using model of figure 7

FIG. 10. Comparing the migrated section when using a) the Marmousi model and b) the inverted model of figure 7. The result of the inverted model is very similar to the one on figure 3d.

Impedance inversion

Impedance inversion is applied according to equation 14 for each monochromatic gradient before. However the resulting gradient is phase shifted. Margrave et al. (2010) computed the required phase rotation by least squares minimization using well log as reference.We compute the least square minimization comparing pilot shot with a synthetic one. The gradient is then converted from depth to time, phase shifted and converted back to depth. After the scale factor is applied and the monochromatic gradients are averaged and the conjugate gradient is computed before the model update.

The inverted model of figure 11 is promising with great potential to be improved, but we could not have an inversion with the same quality of the ones that used scaled reflection coefficients contrasts. Some of the main structures were inverted and the most impressive observation is the inversion of the thick high velocity bodies. Apparently, the use of impedance inversion is a good solution in areas with large continuous structures.

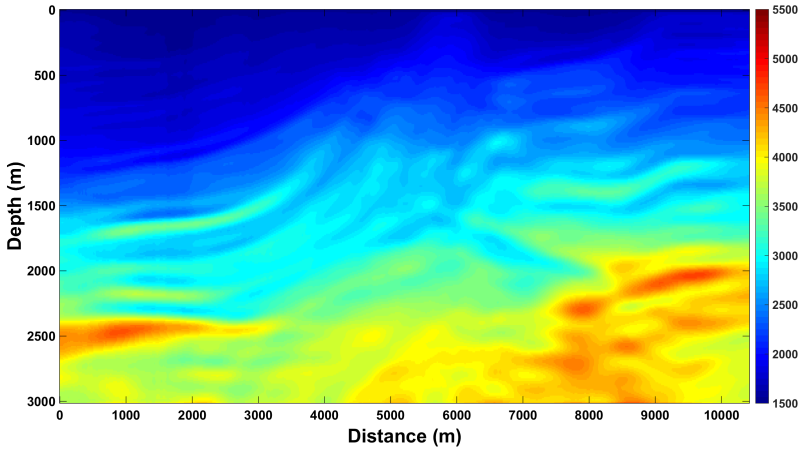

FIG. 11. Inverted model using the conjugate gradient and impedance inversion. The initial guess is the one on figure 3c. Even the inversion been better than the initial guess, It is easy to see that there is a big possibility for improvement.

We believe that the main reason for the inversion had converged to a local minimum is

due to the phase rotation. We compute the necessary phase by comparing pilot shot with synthetic shot in time. Maybe a more sophisticated strategy is required.

According to our results, the usage of reflection coefficients to update the model apparently works better than applying an impedance inversion in the gradient. As discussed above, the impedance inversion requires a phase rotation, while the reflection coefficients seems to be in phase. Also, for very low frequencies, reflection coefficients and impedance are, approximately, differed only by a phase rotation. Our inversion aways take use of low frequencies at each iteration. We starting migrating from $2Hz$ and only maximum frequency is changed. We choose this strategy to keep the trend of the model on every iteration and we enhance the resolution as we increase maximum frequency in the migration step.

CONCLUSIONS

A FWI routine using PSPI migration to compute the gradient was tested on an acoustic synthetic survey as an improvement of the previous work (Guarido et al., 2014). Averaging the scaled monochromatic gradients showed to be a a stable great improvement on estimating the model update, with increased quality of the inverted velocity. This method was possible due the cheaper calculation of the step length if compared with a line search.

Different initial guesses were tried to see the behavior of the FWI routine on each case. We can conclude that closer the start model is to the global minimum, better will be the inverted velocity model. This can be explained by the quality of the migration starting from the first iteration. Interfaces are migrated closer to the correct position and inversion has a higher change to converge to the global minimum.

Including the conjugate gradient step improved the inversion result. Routine got longer to be truncated by the stopping criteria if compared with the classic one. The conjugate gradient took more advantage of the updates and showed steepest decrease of the errors on higher frequencies.

An impedance inversion with a phase rotation correction in time showed promising results, where thick bodies were better "filled" than the reflection coefficients updates, but still need some improvements on the phase rotation step.

ACKNOWLEDGEMENTS

The authors thank the sponsors of CREWES for continued support. This work was funded by CREWES industrial sponsors and NSERC (Natural Science and Engineering Research Council of Canada) through the grant CRDPJ 461179-13. We thank Gary Margrave and Soane Mota dos Santos for the suggestions, tips and productive discussions, and Babatunde Arenrin for providing the step length estimation code.

REFERENCES

Bishop, T. N., and Spongberg, M. E., 1984, Seismic tomography: A case study: SEG Technical Program Expanded Abstracts, **313**, 712–713.

Cutler, R. T., Bishop, T. N., Wyld, H. W., Shuey, R. T., Kroeger, R. A., Jones, R. C., and Rathbun, M. L., 1984, Seismic tomography: Formulation and methodology: SEG Technical Program Expanded Abstracts, **312**, 711–712.

Fatti, J. L., Smith, G. C., Vail, P. J., Strauss, P. J., and Levitt, P. R., 1994, Detection of gas in sandstone reservoirs using avo analysis: A 3-d seismic case history using the geostack technique: Geophysics, **59**, No. 9, 1362–1376.

Ferguson, R., and Margrave, G., 2005, Planned seismic imaging using explicit one-way operators: Geophysics, **70**, No. 5, S101–S109.

Guarido, M., Lines, L., and Ferguson, R., 2014, Full waveform inversion - a synthetic test using the pspi migration: CREWES Research Report, **26**, 26.1–26.23.

Guarido, M., Lines, L., and Ferguson, R., 2015, Full waveform inversion: a synthetic test using pspi migration: SEG Technical Program Expanded Abstract, **279**, 1456–1460.

Lailly, P., 1983, The seismic inverse problem as a sequence of before stack migrations: Conference on inverse scattering, theory and application: Society of Industrial and Applied Mathematics, Expanded Abstracts, 206–220.

Langan, R. T., Lerche, I., Cutler, R. T., Bishop, T. N., and Spera, N. J., 1984, Seismic tomography: The accurate and efficient tracing of rays through heterogeneous media: SEG Technical Program Expanded Abstracts, **314**, 713–715.

Lindseth, R. O., 1979, Synthetic sonic logs-a process for stratigraphic interpretation: Geophysics, **44**, No. 1, 3–26.

Ma, Y., Hale, D., Meng, Z. J., and Gong, B., 2010, Full waveform inversion with image-guided gradient: SEG Technical Program Expanded Abstracts, **198**, 1003–1007.

Margrave, G., Ferguson, R., and Hogan, C., 2010, Full waveform inversion with wave equation migration and well control: CREWES Research Report, **22**, 63.1–63.20.

Margrave, G., Yedlin, M., and Innanen, K., 2011, Full waveform inversion and the inverse hessian: CREWES Research Report, **23**, 77.1–77.13.

Pica, A., Diet, J. P., and Tarantola, A., 1990, Nonlinear inversion of seismic reflection data in a laterally invariant medium: Geophysics, **55**, No. 2, R59–R80.

Pratt, R. G., Shin, C., and Hick, G. J., 1998, Gauss-newton and full newton methods in frequency-space seismic waveform inversion: Geophysical Journal International, **133**, No. 2, 341–362.

Shuey, R. T., 1985, A simplification of the zoeppritz equations: Geophysics, **50**, No. 4, 609–614.

Tarantola, A., 1984, Inversion of seismic reflection data in the acoustic approximation: Geophysics, **49**, No. 8, 1259–1266.

Treitel, S., Lines, L., and Ruckgaber, G., 1995, Seismic impedance estimation: Geophysical Inversion and Applications - Memorial University of Newfoundland, **1**, 6–11.

Vigh, D., and Starr, E. W., 2008, 3d prestack plane-wave, full-waveform inversion: GEOPHYSICS, **73**, No. 5, VE135–VE144.

Virieux, J., and Operto, S., 2009, An overview of full-waveform inversion in exploration geophysics: Geophysics, **74**, No. 6, WCC1–WCC26.

Warner, M., and Guasch, L., 2014, Adaptive waveform inversion: Theory: SEG Technical Program Expanded Abstracts, **207**, 1089–1093.

Wenyong, P., Margrave, G., and Innanen, K., 2013, On the role of the deconvolution imaging condition in full waveform inversion: CREWES Research Report, **25**, 72.1–72.19.

Zhou, C., Cai, W., Luo, Y., Schuster, G. T., and Hassanzadeh, S., 1995, Acoustic wave-equation traveltime and waveform inversion of crosshole seismic data: GEOPHYSICS, **60**, No. 3, 765–773.